Differences in nasal and temporal responses of the cornea after photorefractive keratectomy

Sebastiano Serrao, MD, PhD, Giuseppe Lombardo, Eng, PhD, Marco Lombardo, MD

Purpose: To examine the differences in the biomechanical response of the peripheral regions of the cornea after photorefractive keratectomy (PRK).

Setting: Department of Ophthalmology, Catholic University of Rome, Rome, Italy.

Methods: Preoperative and 1-, 3-, 6-, and 12-month postoperative corneal topographies of 70 eyes that had PRK with the Technolas 217C excimer laser (Bausch & Lomb) were obtained. The eyes were divided into 4 groups according to the preoperative spherical equivalent refraction. Preoperative and follow-up topographic data were imported into custom software that computed the average composite corneal map and difference maps in each group to scientifically evaluate the corneal response to the surgery. The software was also used to analyze regional corneal changes after the laser ablation. Corneal peripheries up to 9.0 mm were evaluated.

Results: The preoperative corneas had a flatter nasal periphery than temporal periphery. The corneal surfaces in the right eyes and left eyes showed a mirror symmetry. Significant differences in the regional response of the cornea were observed ($P < .05$), with a greater increase in the curvature of the nasal periphery than in the temporal periphery.

Conclusions: To refine modeling of the cornea, the different regional anatomic features and biomechanical responses must be considered. Modifying existing ablation algorithms to compensate for the differences between nasal and temporal corneal flattening of the preoperative corneal surface and between the nasal and temporal responses may improve the postoperative corneal shape and quality of peripheral optics.

J Cataract Refract Surg 2005; 31:30–38 © 2005 ASCRS and ESCRS

Since their introduction, radial keratotomy and refractive corneal laser surgery have been developed empirically without detailed knowledge of intrinsic corneal behavior.[1] Refractive surgery, however, stimulated ophthalmologists and researchers to seek understanding of the biomechanical properties of the human cornea. It is now thought that the cornea will accept only certain shapes and that this can be achieved by respecting the normal regional properties of the cornea.[2]

To date, a single identical ablation pattern has been used to treat both the right eye and left eye. The assumption was to treat the cornea as a symmetric lens, subtracting tissue with the widest possible ablation zone.[3] It is well known the corneal plane is normally a prolate asphere[4]; nevertheless, it is not taken into consideration that the eccentricity values along the nasal and temporal meridians of the cornea are not identical.[5] The degree of flattening from the center to the periphery of the corneal surface (negative asphericity)[6] is greater along the nasal meridians than along the temporal ones.[7] In addition, corneal topography of

Accepted for publication September 15, 2004.

From the Department of Ophthalmology, Catholic University of Rome (Serrao, M. Lombardo), Rome, and Liquid Crystal Laboratory, INFM Research Unit of Calabria, Department of Physics, University of Calabria (G. Lombardo), Rende (CS), Italy.

None of the authors has a financial or proprietary interest in any material or method mentioned.

Reprint requests to Sebastiano Serrao, MD, PhD, Via Orazio 31, 00193 Rome, Italy. E-mail: serrao@serraolaser.it.

0886-3350/05/$-see front matter
doi:10.1016/j.jcrs.2004.10.026

normal eyes shows a mirror symmetry[8,9]; therefore, it may be necessary for the algorithm treatment plan to maintain this natural binocular geometrical and optical structure of the cornea.

The normal human cornea has different regional properties. Studies of the cornea's microstructure show its highly heterogeneous nature.[10] In the normal human cornea, the collagen fibrils have a different orientation depending on the specific region and corneal layer. At the limbus, the fibrils have a circular arrangement tangential to the limbus, yielding a ring-shaped structure. In the stroma, the collagen fibrils run preferentially in a vertical and horizontal direction, forming a grid-like structure.[11] This arrangement is more regular in the posterior stroma than in the anterior stroma.

Regional corneal thickness measurements and relationships between refractive and topographic parameters have been reported.[12,13] The authors of these studies found that the thinnest site on the cornea is most commonly in the inferotemporal quadrant, followed by the superotemporal, inferonasal, and superonasal quadrants. They also found that high levels of myopia correlate with a steeper central corneal curvature.

In addition to the anatomic differences, regional biomechanical differences exist. The parts of the human cornea strain differently when exposed to the same intraocular pressure load. The differences in regional corneal strain may be caused by a real difference in corneal elasticity or by regional differences in the corneal stress level.[14] The anterior stroma is less hydrated than the posterior stroma and appears to be stiffer, with stronger junctions between collagen lamellas.[15] It has been postulated that interlamellar cross-links, which are preferentially distributed in the anterior one third and periphery of the stroma, contribute to the regional differences in lamellar shearing strength and interlamellar cohesive strength in the human cornea.[16,17] Studies of the differences in the regional laser–tissue interactions[18,19] found the corneal periphery has a greater decrease in ablation depth per laser pulse (cut rate) than the central corneal zone.

Both the regional lamellar strength differences and asymmetric epithelial healing may contribute to a different nasal and temporal response of the cornea after photorefractive keratectomy (PRK). An increased knowledge of the regional differences of the cornea could lead to better prediction of the corneal response after a refractive procedure and to a decrease in induced high-order optical aberrations. Although the biomechanical response of the cornea can influence the ultimate optical aberrations of the eye, it cannot be predicted using a wavefront approach.[20] Detailed knowledge of corneal biomechanics will help us understand how some biomechanical changes of the cornea can be determined and thus be predicted more easily, allowing ophthalmic researchers and laser manufacturers to develop new ablation algorithms to predict and correct unwanted biomechanical and optical changes.

In a previous paper,[21] we noted that the temporal and nasal changes during epithelial healing after PRK are different. In the present study, we report data from the preoperative and the postoperative corneal topographies of 70 eyes that had PRK for the correction of myopia or astigmatism. The aim was to investigate the differences in the local curvature and biomechanical response between the nasal and temporal zones of the corneal surface after PRK.

Materials and Methods

Thirty-five patients (70 eyes) were enrolled in this prospective randomized study. The inclusion criterion was a manifest spherical equivalent (SE) refraction from −2.00 to −8.00 diopters (D). The exclusion criteria were systemic or ocular disease or previous ocular surgery. Patients wearing contact lenses were asked to discontinue their use at least 4 weeks before surgery. All patients provided informed consent.

The eyes were divided into 4 groups depending on the SE refraction (Table 1): low myopia (range −2.00 to −3.60 D), moderate myopia (range −3.70 to −5.60 D), high myopia (range −5.70 to −8.00 D), and astigmatism (with the rule [WTR]; range −1.75 to −5.00 D). In the 3 simple myopia groups, the cylinder component was no greater than 1.00 D.

The PRK procedure was performed with a Technolas Keracor 217C excimer laser (Bausch & Lomb) using an ablation zone of 6.0 mm, a transition zone up to 9.0 mm, and an active eye-tracker device. The astigmatism group was treated with a cross-cylinder technique[22]; hyperopic photorefractive astigmatic keratectomy (PARK) and myopic PARK were performed with a 6.0 mm ablation zone and a 3.0 mm transition zone.

Phototherapeutic keratectomy (PTK) was performed using the smoothing technique,[23] in which a viscous masking solution of sodium hyaluronate 0.25% is used at the end of the procedure. The laser was set in PTK mode and the ablation depth, at 10 μm. The masking fluid was

Table 1. Preoperative and 1-year postoperative SE refraction in the right eyes and left eyes in the 4 study groups.

	Mean SE Refraction (D) ± SD			
Exam	**Low Myopia Group**	**Moderate Myopia Group**	**High Myopia Group**	**Astigmatism Group**
Preoperative				
Both eyes	−2.84 ± 0.81	−4.43 ± 0.54	−6.95 ± 0.83	−4.21 ± 2.42
Right eye	−2.95 ± 0.80	−4.38 ± 0.52	−7.20 ± 0.87	−3.79 ± 2.83
Left eye	−2.71 ± 0.84	−4.48 ± 0.53	−6.70 ± 0.77	−4.71 ± 2.07
Postoperative				
Both eyes	+0.03 ± 0.28	−0.03 ± 0.30	+0.12 ± 0.35	−0.75 ± 0.83
Right eye	+0.04 ± 0.29	+0.02 ± 0.31	+0.28 ± 0.38	−0.83 ± 1.05
Left eye	−0.00 ± 0.27	−0.01 ± 0.27	−0.04 ± 0.24	−0.64 ± 0.58

SE = spherical equivalent

spread over the corneal surface with a spatula. A new drop of the viscous substance was added at the center of the corneal surface and spread with the spatula when dry areas were exposed.

Postoperatively, patients were prescribed preservative-free micronomycin eyedrops 6 times daily until complete reepithelialization of the cornea, topical fluorometholone 0.10% twice daily for 1 month after complete reepithelialization, and preservative-free sodium hyaluronate 0.18% hypotonic solution eyedrops 5 times daily for 6 months after surgery.

All patients had a complete ocular evaluation preoperatively and after 1, 3, 6, and 12 months postoperatively. The examination included corneal topography using the Keratron Scout (Optikon 2000),[24] which is based on the Placido ring method.[25] The area of analysis was 140 mm^2; the maximum corneal coverage in a normal eye is 11.0 mm with 90% of the corneal surface measured. The large surface coverage is due the instrument's cone, which is small and very close to the eye.

To acquire information on the corneal regional behavior properties, a power topographic software tool was developed in accordance with a previously described system.[26] The software can analyze differences in the curvature of the peripheral corneal zones and the modifications occurring after surgery.

The preoperative and postoperative topographic data were exported using custom software for detailed evaluation of the numerical data from the corneal maps. The software was written in Matlab (version 6.5, MathWorks, Inc.), a commercial scientific computing and visualization environment for numerical modeling and data analysis. It has high-language syntax, a mathematical library software, and integrated graphics. The Matlab graphics library and a code from its basic function suite ("griddata" function) have been used to interpolate the irregularly sampled raw cornea data geometry to the regularly spaced referenced cornea grid.[27] The custom software was used to export the geometry and curvature data processed from a corneal image of 28 rings and 256 meridians, as done with the measuring device.

To process these data correctly, it was necessary to interpolate the raw curvature and elevation map data for each patient's eye to a regularly spaced referenced corneal grid, eliminating the dependents among the single topographies. The reference cornea grid had 300 meridians and 100 rings, all equally spaced. The corneal reference frame was divided into 2 concentric regions: the inner region, with a radius 3.0 mm from the corneal apex, and the outer region, with a radius 4.5 mm from the apex. This allowed separate analysis of the central corneal surface and the peripheral corneal surface. The reference cornea grid was further divided into 4 zones (inner nasal, outer nasal, inner temporal, and outer temporal) to highlight the preoperative and postoperative differences between the zones and to better characterize the regional responses of the cornea after laser ablation (Figure 1).

The mathematical algorithm software computed the average preoperative and postoperative tangential curvature map and average elevation map with respect to the reference axis for the right and left eyes in each study group. It also computed an average tangential curvature difference map (postoperatively at 1, 3, 6, and 12 months minus preoperatively). For the elevation maps, the preoperative and postoperative surfaces were fitted tangentially to the apex. Tilts between the corneal elevations were avoided by aligning the data with one another, which required interpolation to the same spaced referenced cornea grid. A "fixed" color scale was developed for rapid and easy interpretation.

The differences between the postoperative and preoperative tangential curvatures of the nasal and temporal outer regions in each study group were compared using the analysis of variance (ANOVA) procedure in the statistical toolboxes of Matlab.

Results

The study comprised 15 men and 20 women with a mean age of 31.7 years ± 5.95 (SD) (range 25 to 45 years). There were no statistically significant

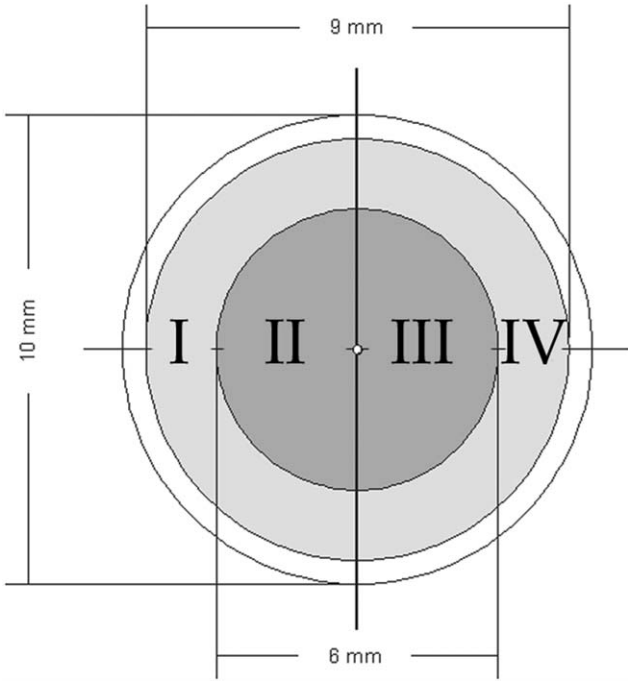

Figure 1. The cornea reference frame (10.0 mm in diameter) was divided into 2 concentric regions for regional topographic data analysis. The innermost circle defines the inner region, which has a radius 3.0 mm from the corneal apex, and the central circle defines the outer region, which has a radius 4.5 mm from the apex. The reference cornea grid was further divided in 4 zones (I, II, III, and IV) for nasal and temporal analysis.

differences in the preoperative SE refraction between the right eye and fellow left eye in any of the 4 study groups ($P > .05$, Fisher test) (Table 1).

The preoperative central corneal curvature values were not significantly different between the groups. The peripheral values were lower depending on the degree of refractive error. In all groups, the nasal regions had a lower radius of curvature than the temporal regions (Table 2).

As expected, postoperative central flattening and peripheral steepness correlated well with the degree to which the refractive error was corrected. Table 3 shows the numerical results for each corneal zone in the right eyes and left eyes in the 4 groups. Figure 2 shows the average composite map of the right eyes and left eyes before surgery and at 1 year in the low myopia group.

At each follow-up evaluation, typical asymmetry between the nasal and temporal eccentricities was observed. Although it could be thought the pattern was not central, the difference maps at each follow-up showed the treatments were well centered. Figures 3 and 4 show the average composite difference maps in the 2 simple myopia groups.

For cross-cylinder treatment, the hyperopic toric ablation cut tissue in a more peripheral zone of the cornea and the differences in local curvature asymmetry between the nasal and temporal peripheral regions after the ablation were more consistent than with the spherical ablations. Furthermore, at the end of follow-up, the astigmatism was fully corrected in the inner region of the cornea, while a more marked asymmetry was created in the outer region. Figure 5 and Figure 6 show the average tangential composite maps and the average composite difference maps, respectively, in the astigmatism group.

Figure 7 shows the color data analysis of the corneal regions performed by the software for the left eyes in the astigmatism group. The central region emphasizes the changes within the optical zone, and the outer region emphasizes the changes outside the optical zone. These changes were thus related to the biomechanical response of the cornea.

Narrowing of the optical zone during follow-up was noted, especially in the high myopia group. This was associated with a change in the curvature of the peripheral zones (Figure 8).

Nevertheless, in the ablated corneas, the eccentricity values decreased to oblate values and the nasal zone changes were more pronounced than the temporal changes ($P < .05$, ANOVA). The differences in regional peripheral curvature were similar to the preoperative values, with the nasal peripheral zones showing a lower radius of curvature than the temporal zones. Furthermore, the deeper and more peripheral the laser ablation, the greater the increase in the curvature difference between the nasal and temporal peripheral zones. In addition, greater variability in peripheral curvature changes after the laser ablation was observed in the high myopia and astigmatism groups (Table 3).

Discussion

The curvatures of the normal right and left human corneas show a mirror symmetry. The eccentricity varies along the corneal nasal or temporal meridians; the increase in flattening is more consistent along the nasal zones of the cornea. The laser ablation pattern

Table 2. Mean preoperative local curvature of the nasal and temporal corneal zones obtained from the software system.

	Mean Curvature (D) ± SD			
Corneal Zone	**Low Myopia Group**	**Moderate Myopia Group**	**High Myopia Group**	**Astigmatism Group**
Right eye				
C–N	43.37 ± 0.85	44.07 ± 0.98	43.22 ± 0.82	44.07 ± 1.78
C–T	43.78 ± 0.56	44.54 ± 0.67	43.50 ± 0.66	44.76 ± 1.31
O–N	37.06 ± 4.50	38.31 ± 3.95	35.78 ± 6.60	35.29 ± 5.30
O–T	40.04 ± 2.11	40.55 ± 2.06	39.92 ± 3.07	39.43 ± 3.50
Left eye				
C–N	43.21 ± 0.96	43.67 ± 0.91	43.73 ± 1.05	43.91 ± 1.47
C–T	43.52 ± 0.43	44.01 ± 0.50	44.26 ± 0.41	44.72 ± 0.91
O–N	36.81 ± 4.55	38.02 ± 3.52	35.94 ± 5.70	36.54 ± 5.76
O–T	40.32 ± 2.41	40.55 ± 2.03	39.56 ± 2.74	41.59 ± 4.46

C = inner; N = nasal; O = outer; T = temporal

does not take into account the differences between the nasal and temporal regions in the increase in flattening from the apex to the periphery.

We specifically noted that the corneal response in the nasal zones was different than that in the temporal zones, with a greater increase in curvature outside the area of ablation in the nasal peripheral regions than in the temporal regions.

In the low myopia group, the nasal–temporal difference in eccentricity values changed slightly after the laser ablation. Marked induced asymmetry was observed in the astigmatism group. We believe the greater induced asymmetry observed after the astigmatic ablation may be correlated with the more peripheral ablation pattern and the different biomechanical properties of the periphery of the corneal plane. The more peripheral the ablation, as in hyperopic treatments, the more corneal surface asymmetry the laser will encounter and the greater the difference in the regional response of the cornea.

The greater peripheral response in the high myopia group could be related to the different biomechanical properties between the posterior stroma and the anterior stroma. Stiffer stroma, such as that in the

Table 3. Mean anterior tangential regional differences (postoperative minus preoperative) for right eyes and the left eyes 1 year after surgery.*

	Mean Difference (D) ± SD			
Corneal Zone	**Low Myopia Group**	**Moderate Myopia Group**	**High Myopia Group**	**Astigmatism Group**
Right				
C–N	−1.03 ± 1.27	−2.81 ± 2.45	−3.29 ± 4.80	−3.34 ± 1.38
C–T	−1.36 ± 1.05	−2.25 ± 2.48	−3.07 ± 3.35	−2.45 ± 1.32
O–N	3.16 ± 3.14	5.44 ± 2.01	5.90 ± 6.90	5.38 ± 7.04
O–T	1.99 ± 1.97	4.09 ± 1.10	5.10 ± 6.10	1.92 ± 3.77
Left				
C–N	−1.25 ± 1.10	−2.81 ± 2.03	−3.09 ± 3.34	−3.43 ± 1.37
C–T	−1.06 ± 0.87	−2.60 ± 1.74	−3.27 ± 4.61	−2.52 ± 1.19
O–N	2.96 ± 2.29	4.22 ± 1.73	6.65 ± 5.50	2.36 ± 5.13
O–T	2.06 ± 1.35	3.86 ± 1.67	5.90 ± 6.95	1.78 ± 3.53

C = inner; N = nasal; O = outer; T = temporal
*$P < .05$, ANOVA

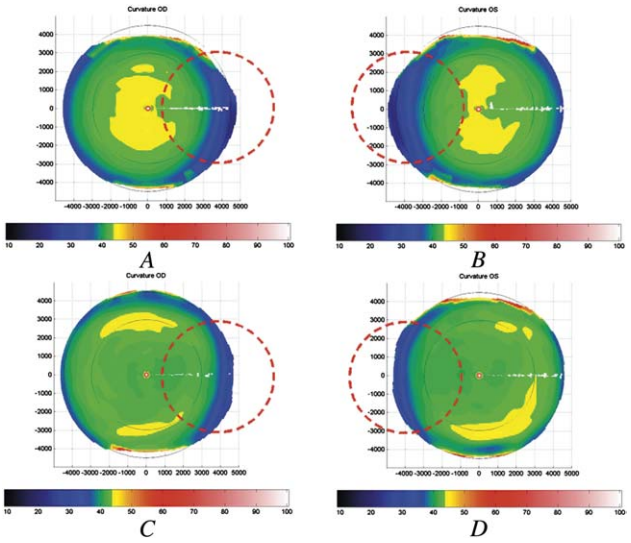

Figure 2. Tangential curvature maps in the low myopia group. The faint black circles surrounding the topography define 2 corneal regions. The central region has a 3.0 mm radius and the outer region, a 4.5 mm radius. The preoperative average composite maps of the right eye (*A*) and left eye (*B*) show differences in corneal flattening, moving from the center to the periphery, between the nasal and the temporal meridians (red-dotted circle on right [*A*, *C*] or left [*B*, *D*] of the topography). The 1 year postoperative average composite maps (*C* and *D*) have an asymmetric surface pattern similar to the surface in the preoperative maps (color-scale bar = diopters).

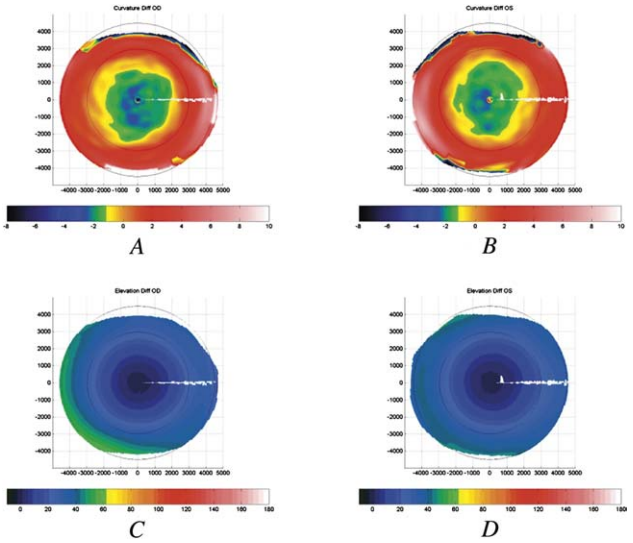

Figure 3. Difference maps (1 year postoperative minus preoperative) in the low myopia group. The top row shows the tangential curvature difference maps of the right eye (*A*) and left eye (*B*). Note the asymmetric nasal–temporal increase in curvature of the regions outside the ablation (scale color bar = diopters). The bottom row shows the elevation difference maps of the right eye (*C*) and left eye (*D*). The ablation pattern is regular in both eyes (color-scale bar = microns).

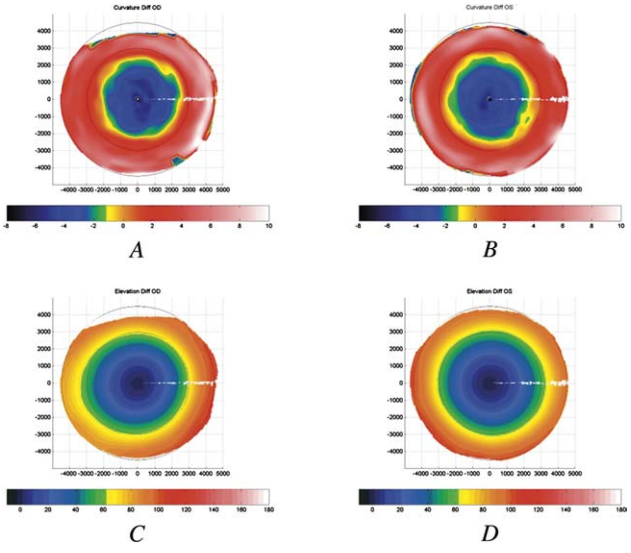

Figure 4. Difference maps (1 year postoperative minus preoperative) in the moderate myopia group. The top row shows the tangential curvature difference maps of the right eye (*A*) and left eye (*B*). The nasal–temporal asymmetric response of the regions outside the ablation is more pronounced than in the low myopia group (color-scale bar = diopters). The bottom row shows the elevation difference maps of the right eye (*C*) and left eye (*D*). Note the regular ablation pattern for both eyes and the deeper ablation compared with the ablation in the low myopia group (color-scale bar = microns).

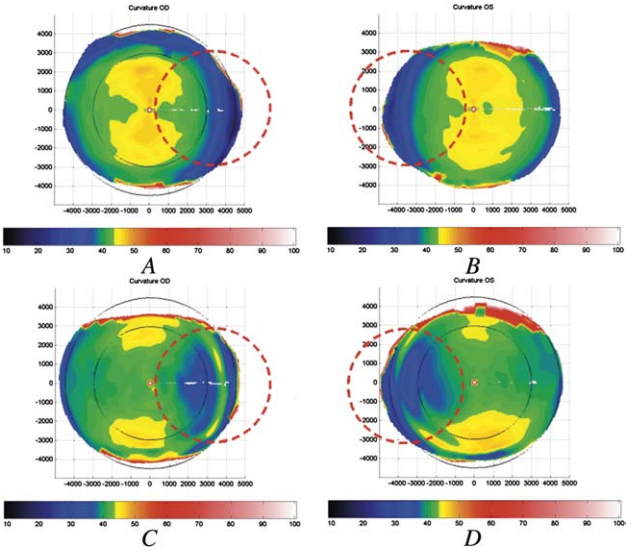

Figure 5. Tangential curvature maps in the astigmatism group. The preoperative average composite maps both of the right eye (*A*) and the left eye (*B*) show regular WTR astigmatism. Differences in corneal flattening from the apex to the periphery between the nasal and temporal meridians (red-dotted circle on right [*A*, *C*] or left [*B*, *D*] of the topography) are also seen. The 1-year postoperative average composite maps of the right eye (*C*) and left eye (*D*) show the less astigmatism in the inner region due to the cross-cylinder ablation and an increase in curvature differences between the nasal and temporal peripheral zones compared with the preoperative state (color-scale bar = diopters).

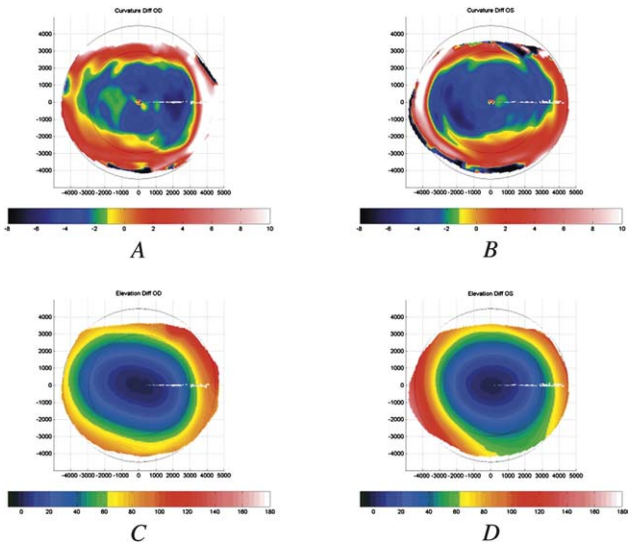

Figure 6. Difference maps (1 year postoperative minus preoperative) in the astigmatism group. The top row shows the tangential curvature difference maps for the right eye (*A*) and left eye (*B*). There is decreased curvature along the horizontal peripheral meridians due to the hyperopic toric ablation, and the nasal region is flattener than the temporal region. The increase in the curvature of the nasal region outside the ablation is more marked than the increase in the temporal region (color scale bar = diopters). The bottom row shows the elevation difference maps of the right eye (*C*) and left eye (*D*). Note the toric axis-symmetric ablation pattern in both eyes (color scale bar = microns).

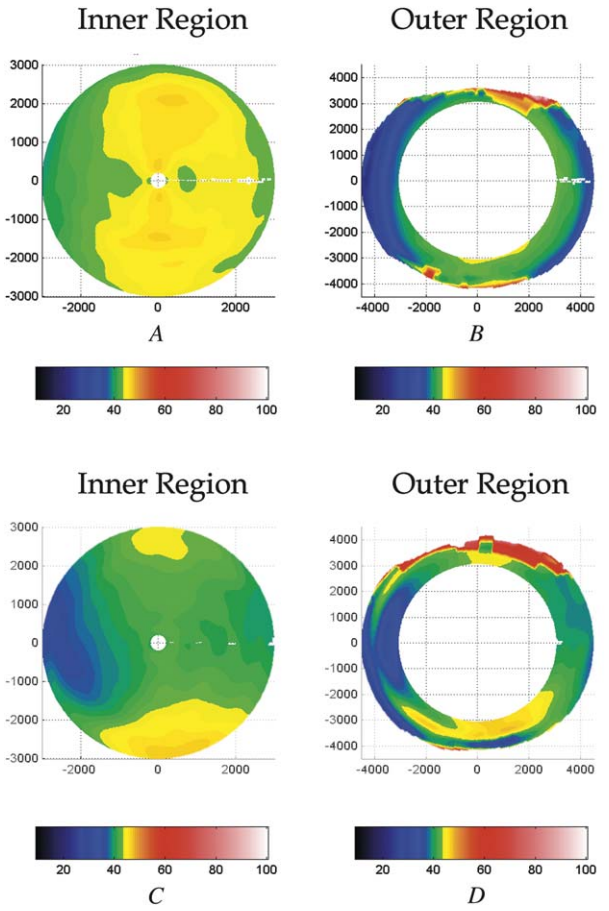

Figure 7. Average tangential curvature maps of the left eye in the astigmatism group. The software was used to divide the corneal topography into 2 concentric regions. The inner region has a radius 3.0 mm from the corneal apex and the outer region, 4.5 mm from the apex. The upper row shows the preoperative maps of the inner region (*A*) and the outer region (*B*). The lower row shows the 1-year postoperative maps of the inner region (*C*) and outer region (*D*) (color-scale bar = diopters).

anterior region, could have a modest response. The high myopia group and the astigmatism group had greater variability in increased curvature changing in the region outside the ablation than the other groups. This could be related to the amount of tissue removed and to the more peripheral ablation, respectively.

Other authors[18,19,28] report how the effect of corneal surface inclination on the effective fluence and tissue ablation rates of the incoming laser beam, as well as the obliquity of incident radiation falling on peripheral cornea, may result in decreased energy density to the outer parts of the treatment zone. For this reason, we believe a difference in the ratio of absorbed laser light versus reflected laser light could also produce ablations of different depths in the nasal cornea versus the temporal cornea due to local asphericity changes, resulting in an asymmetric response.

The smoothing technique has been shown to be a safe procedure.[23] It could not have induced a consistent corneal response because of the very small amount of tissue removed and the symmetric distribution of the masking fluid on the cornea.[29]

Finally, the observed corneal changes demonstrate how the biophysical remodeling of the cornea is not yet complete 1 year after surgery. Although it is reasonable that the later changes may be epithelial in nature,[30] we emphasize that the immediate topographic regional differences are biomechanical in nature.

The local differences in the normal human cornea must be included in the preoperative data as they could influence surgical technique and calculation of the ablation algorithm. In fact, it is known that the Bowman's layer plays no particular role in the elastic response of the cornea after PRK,[31] whereas the flap in laser in situ keratomileusis (LASIK) introduces many preablation variables depending on the depth of the

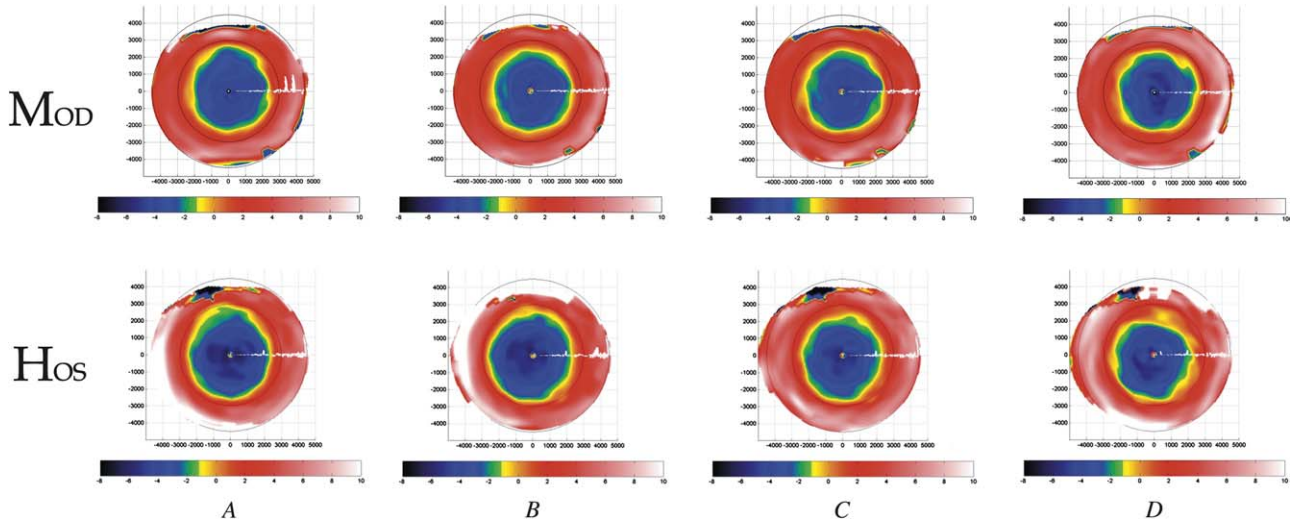

Figure 8. Tangential curvature difference maps of the right and left eyes in the moderate myopia group (MOD) and high myopia group (HOS) during follow-up. *A*: One-month postoperative map minus preoperative map. *B*: Three-month postoperative map minus preoperative map. *C*: Six-month postoperative map minus preoperative map. *D*: Twelve-month postoperative minus preoperative map. Note the narrowing of the optical zone and the curvature changes in the regions outside the ablation during the follow-up.

incision, the location and size of the hinge, and flap uniformity.[32] Thus, the LASIK flap may increase the regional asymmetry of the cornea and the postablation corneal changes in PRK may be more predictable. The ablation algorithm must take into account the different degrees of corneal flattening along the nasal meridians compared with the temporal meridians and the mirror symmetrical curvature of the right eye and left eye.

Performing an axis-symmetric ablation on the normal cornea invariably leads to asymmetry similar to or greater than that of the preoperative cornea. Our data show that ablation of the nasal and temporal regions of the same cornea, which have different microstructural and biomechanical properties, leads to a different regional response.

In addition, a difference in the nasal–temporal eccentricity between the right eyes and left eyes results in a mirror symmetry of high-order aberrations.[8] Not to consider this optical asymmetry between eyes in the treatment plan could lead to underestimation of a variable of induction of high-order aberrations and an unpredictable biomechanical response.

The clinical implications of this study could have an impact on the strategies used in laser refractive surgery. The corneal response after laser ablation is still a considerable problem. Our results show that in a normal cornea, the nasal zones are flatter than the temporal ones and that these regions have different biomechanical properties; therefore, it is reasonable to select an ablation approach on the basis of these curvature differences between eyes. Future nomograms cannot be based only on factors such as refractive error and age. Corneal topography is needed to further refine the surgical procedure and improve visual outcomes and thus is an essential component of the treatment plan. The incorporation of the morphological changes induced in the cornea after ablation is the next step in the evolution of refractive surgery.

The software system we used permitted us to scientifically characterize the local response of the cornea to different laser ablation patterns. Furthermore, our research will help us understand how some of the biomechanical changes of the cornea can be determined and hence be more predictable. Knowledge of the interindividual similarities in the features of the corneal surface could allow more precise prediction of the corneal biomechanical response. Nevertheless, customization requires prediction of the individual rather the mean corneal response. As Roberts[33] pointed out in 2000, customized laser ablation does not resolve this problem; a linear correction factor may not be sufficient to account for the biomechanical effects. Further topographic investigations are required to develop more accurate topographic- and wavefront-guided procedures.[34]

References

1. Buzard KA. Introduction to biomechanics of the cornea. Refract Corneal Surg 1992; 8:127–138
2. Roberts C. The cornea is not a piece of plastic [editorial]. J Refract Surg 2000; 16:407–413
3. Munnerlyn CR, Koons SJ, Marshall J. Photorefractive keratectomy: a technique for laser refractive surgery. J Cataract Refract Surg 1988; 14:46–52
4. Bogan SJ, Waring GO III, Ibrahim O, et al. Classification of normal corneal topography based on computer-assisted videokeratography. Arch Ophthalmol 1990; 108:945–949
5. Preussner PR, Wahl J, Kramann C. Corneal model. J Cataract Refract Surg 2003; 29:471–477
6. Eghbali F, Yeung KK, Maloney RK. Topographic determination of corneal asphericity and its lack of effect on the refractive outcome of radial keratotomy. Am J Ophthalmol 1995; 119:275–280
7. Rowsey JJ, Balyeat HD, Monlux R, et al. Prospective evaluation of radial keratotomy; photokeratoscope corneal topography. Ophthalmology 1988; 95:322–334
8. Wang L, Dai E, Koch DD, Nathoo A. Optical aberrations of the human anterior cornea. J Cataract Refract Surg 2003; 29:1514–1521
9. McKendrick AM, Brennan NA. The axis of astigmatism in right and left eye pairs. Optom Vis Sci 1997; 74:668–675
10. Komai Y, Ushiki T. The three-dimensional organization of collagen fibrils in the human cornea and sclera. Invest Ophthalmol Vis Sci 1991; 32:2244–2258
11. Meek KM, Blamires T, Elliott GF, et al. The organisation of collagen fibrils in the human corneal stroma: a synchroton x-ray diffraction study. Curr Eye Res 1987; 6:841–846
12. Liu Z, Huang AJ, Pflugfelder SC. Evaluation of corneal thickness and topography in normal eyes using the Orbscan corneal topography system. Br J Ophthalmol 1999; 83:774–778
13. Budak K, Khater TT, Friedman NJ, et al. Evaluation of relationships among refractive and topographic parameters. J Cataract Refract Surg 1999; 25:814–820
14. Hjortdal JØ. Regional elastic performance of the human cornea. J Biomech 1996; 29:931–942
15. Muller LJ, Pels E, Vrensen GFJM. The specific architecture of the anterior stroma accounts for maintenance of corneal curvature. Br J Ophthalmol 2001; 85:437–443
16. Smolek MK, McCarey BE. Interlamellar adhesive strength in human eyebank corneas. Invest Ophthalmol Vis Sci 1990; 31:1087–1095
17. Smolek MK. Interlamellar cohesive strength in the vertical meridian of human eye bank corneas. Invest Ophthalmol Vis Sci 1993; 34:2962–2969
18. Mrochen M, Seiler T. Influence of corneal curvature on calculation of ablation patterns used in photorefractive laser surgery. J Refract Surg 2001; 17:S584–S587
19. Ginis HS, Katsanevaki VJ, Pallikaris IG. Influence of ablation parameters on refractive changes after photorefractive keratectomy. J Refract Surg 2003; 19:443–448
20. Nagy ZZ, Palágyi-Deák I, Kelemen E, Kovács A. Wavefront-guided photorefractive keratectomy for myopia and myopic astigmatism. J Refract Surg 2002; 18:S615–S619
21. Serrao S, Lombardo M, Mondini F. Photorefractive keratectomy with and without smoothing: a bilateral study. J Refract Surg 2003; 19:58–64
22. Vinciguerra P, Sborgia M, Epstein D, et al. Photorefractive keratectomy to correct myopic or hyperopic astigmatism with a cross-cylinder ablation. J Refract Surg 1999; 15:S183–S185
23. Serrao S, Lombardo M. One-year results of photorefractive keratectomy with and without surface smoothing using the Technolas 217C laser. J Refract Surg 2004; 20:444–449
24. Mattioli R, Tripoli NK. Corneal geometry reconstruction with the Keratron videokeratographer. Optom Vis Sci 1997; 74:881–894
25. Mejía-Barbosa Y, Malacara-Hernández D. A review of methods for measuring corneal topography. Optom Vis Sci 2001; 78:240–253
26. Mahmoud AM, Roberts C, Herderick EE. The Ohio State University Corneal Topography Tool. ARVO abstract 3599. Invest Ophthalmol Vis Sci 2000; 41(4):S677
27. Barber CB, Dobkin DP, Huhdanpaa HT. The Quickhull algorithm for convex hulls. ACM Trans Math Software 1996; 22:469–483
28. Hersh PS, Fry K, Blaker W. Spherical aberration after laser in situ keratomileusis and photorefractive keratectomy; clinical results and theoretical models of etiology. J Cataract Refract Surg 2003; 29:2096–2104
29. Dogru M, Katakami C, Yamanaka A. Refractive changes after excimer laser phototherapeutic keratectomy. J Cataract Refract Surg 2001; 27:686–692
30. Møller-Pedersen T, Cavanagh HD, Petroll WM, Jester JV. Stromal wound healing explains refractive instability and haze development after photorefractive keratectomy; a 1-year confocal microscopic study. Ophthalmology 2000; 107:1235–1245
31. Hjortdal JØ, Ehlers N. Effect of excimer laser keratectomy on the mechanical performance of the human cornea. Acta Ophthalmol Scand 1995; 73:18–24
32. Lipshitz I. Thirty-four challenges to meet before excimer laser technology can achieve super vision. J Refract Surg 2002; 18:740–743
33. Roberts C. Future challenges to aberration-free ablative procedures. J Refract Surg 2000; 16:S623–S629
34. Roberts C. Biomechanics of the cornea and wavefront-guided laser refractive surgery. J Refract Surg 2002; 18: S589–S592